Proceedings of the
International Conference on Mechanical Engineering 2009
(ICME2009) 26- 28 December 2009, Dhaka, Bangladesh

ICME09-FM-03

STUDY ON REAL GAS FLOWS THROUGH A CRITICAL NOZZLE

Mamun Mohammad[1], Junji Nagao[2], Shigeru Matsuo[3], Tokitada Hashimoto[3] and Toshiaki Setoguchi[4]

[1] Dept. of Mechanical Engineering, BUET, Dhaka, Bangladesh.
[2] Graduate School of Science and Engineering, Saga University, Japan
[3] Dept. of Mechanical Engineering, Saga University, Japan.
[4] Institute of Ocean Energy, Saga University, Japan.

ABSTRACT

A critical nozzle is used to measure the mass flow rate of gas. It is well known that the coefficient of discharge of the flow in a critical nozzle is a single function of the Reynolds number. The purpose of the present study is to investigate high-pressure gas flow of air through a critical nozzle. A computational analysis has been carried out to simulate a critical nozzle flow with real gas effects. A modified Berthelot's equation of state is incorporated into the axisymmetric, compressible Navier–Stokes equations. The computational results show that the discharge coefficient for ideal gas assumptions is significantly different from those of the real gas, as the Reynolds number exceeds a certain value. It is also known that the real gas effects appear largely in terms of the compressibility factor and the specific heat ratio, and these become more remarkable as the gas pressure increases. Furthermore, the effects of amplitudes and frequencies of the pressure disturbance on the gas flow through a critical nozzle were investigated numerically.

Keywords: Compressible flow, Critical nozzle, Real gas effects, Discharge coefficient, Simulation.

1. INTRODUCTION

The minimum pressure ratio for the flow to choke is called the critical pressure ratio. Once choked, the flow is no longer dependent on the pressure change in the downstream flow field. In this case, the mass flow is determined only by the stagnation conditions upstream of the flow passage. The critical nozzle is defined as a device to measure the mass flow with only the nozzle supply conditions, making use of the flow-choking phenomenon at the nozzle throat.

In the past, much attention has been paid to the prediction of mass flow through a flow passage, since it was of practical importance in a variety of industrial and engineering fields. The mass flowrate and critical pressure ratio are associated with the working gas consumption and the establishment of safe operation conditions of the critical nozzle. According to previous researches [1-3], the mass flowrate and critical pressure ratio are strong functions of the Reynolds number (*Re*).

Of many kinds of working gases employed in industrial field, it is being recognized that hydrogen gas is one of the most promising gases as a future alternative energy source. In such an application, precise measurement of flowrate is of practical importance for mileage and power output of the vehicle. A large number of works [4–7] has been made to investigate the thermo-physical properties of hydrogen gas, which are specified by some different kinds of the equations of state, the critical pressure, the compressibility factor of hydrogen gas, etc. However, only a few researches have been made to date on the mass flowrate of the high-pressure hydrogen gas through a critical nozzle, due to difficulties of treatment. Recently, Nakao [8] has conducted the flowrate measurement of hydrogen gas using a critical nozzle experimentally. It was shown in the range of high Reynolds number that the coefficient of discharge decreased with an increase of *Re*.

The objectives in the present study are to investigate the flow features of high-pressure air gas through a critical nozzle, with the help of a CFD method and to clarify the effects of amplitudes and frequencies of the pressure disturbance on the gas flow through a critical nozzle numerically. Modified Berthelot's equation of state [9] is employed to consider the force and volume effects of inter-molecules of air gas, and it is incorporated into the axisymmetric, compressible Navier–Stokes equations. Furthermore, the computational results (coefficient of discharge) are validated with some experimental data available.

2. CFD ANALYSIS

2.1 Governing Equations

The governing equations, i.e., the unsteady compressible Navier-Stokes equations written in an axisymmetric coordinate system (x,y) are as follows :

$$\frac{\partial \boldsymbol{U}}{\partial t}+\frac{\partial \boldsymbol{E}}{\partial x}+\frac{\partial \boldsymbol{F}}{\partial y}=\frac{1}{Re}\left(\frac{\partial \boldsymbol{R}}{\partial x}+\frac{\partial \boldsymbol{S}}{\partial y}\right)+\frac{1}{y}\boldsymbol{H}_1+\boldsymbol{H}_2 \quad (1)$$

where

$$\boldsymbol{U}=\begin{bmatrix}\rho\\ \rho u\\ \rho v\\ E_t\\ \rho k\\ \rho\varepsilon\end{bmatrix},\ \boldsymbol{E}=\begin{bmatrix}\rho u\\ \rho u^2+p\\ \rho uv\\ u(E_t+p)\\ \rho ku\\ \rho\varepsilon u\end{bmatrix},\ \boldsymbol{F}=\begin{bmatrix}\rho v\\ \rho uv\\ \rho v^2+p\\ v(E_t+p)\\ \rho kv\\ \rho\varepsilon v\end{bmatrix},$$

$$\boldsymbol{R}=\begin{bmatrix}0\\ \tau_{xx}\\ \tau_{xy}\\ \alpha\\ \left(\mu+\frac{\mu_t}{\sigma_k}\right)\frac{\partial k}{\partial x}\\ \left(\mu+\frac{\mu_t}{\sigma_\varepsilon}\right)\frac{\partial \varepsilon}{\partial x}\end{bmatrix},\ \boldsymbol{S}=\begin{bmatrix}0\\ \tau_{xy}\\ \tau_{yy}\\ \beta\\ \left(\mu+\frac{\mu_t}{\sigma_k}\right)\frac{\partial k}{\partial y}\\ \left(\mu+\frac{\mu_t}{\sigma_\varepsilon}\right)\frac{\partial \varepsilon}{\partial y}\end{bmatrix},$$

$$\boldsymbol{H}_1=\begin{bmatrix}-\rho v\\ \tau_{xy}-\rho uv\\ \alpha-\rho v^2\\ \beta-(E_t+p)v\\ 0\\ 0\end{bmatrix},\ \boldsymbol{H}_2=\begin{bmatrix}0\\ 0\\ 0\\ 0\\ P_k-\rho\varepsilon\\ C_{1\varepsilon}\frac{\varepsilon}{k}P_k-C_{2\varepsilon}\rho\frac{\varepsilon^2}{k}\end{bmatrix} \quad (2)$$

$$E_t=\rho C_p T+\frac{1}{2}\rho\left(u^2+v^2\right) \quad (3)$$

$$p=(\gamma-1)\left[E_t-\frac{1}{2}\rho\left(u^2+v^2\right)\right] \quad (4)$$

$$\alpha=u\tau_{xx}+v\tau_{yx}+\kappa\frac{\partial T}{\partial x},\ \beta=u\tau_{xy}+v\tau_{yy}+\kappa\frac{\partial T}{\partial y} \quad (5)$$

$$\mu_t=\rho C_\mu\frac{k^2}{\varepsilon} \quad (6)$$

$$P_k=2\mu_t\left[\left(\frac{\partial u}{\partial x}\right)^2+\frac{1}{2}\left(\frac{\partial v}{\partial x}+\frac{\partial u}{\partial y}\right)+\left(\frac{\partial v}{\partial y}\right)^2\right] \quad (7)$$

$$C_{1\varepsilon}=1.44,\ C_{2\varepsilon}=1.92,\ C_\mu=0.09,\ \sigma_k=1.0,\ \sigma_\varepsilon=1.3 \quad (8)$$

For air, a modified Berthelot was used to obtain the compressibility factor as follows [9]:

$$p=\frac{RT}{v}\left\{1+\frac{9pT_c}{128p_cT}\left(1-\frac{6T_c^2}{T^2}\right)\right\} \quad (9)$$

p_c and T_c are critical pressure and critical temperature, respectively. In Eq.(2), $\boldsymbol{U}$ is the conservative vector, $\boldsymbol{E}$ and $\boldsymbol{F}$ are inviscid flux vector and $\boldsymbol{R}$ and $\boldsymbol{S}$ are viscous

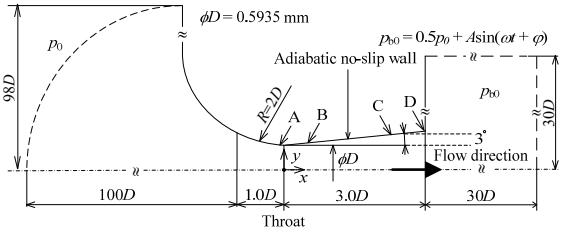

Fig 1. Details of critical nozzle

flux vectors. $\boldsymbol{H}_1$ and $\boldsymbol{H}_2$ are the source terms corresponding to axisymmetry and turbulence, respectively. τ_{xx}, τ_{xy}, τ_{yx} and τ_{yy} are components of viscous shear stress.

Table 1: Initial conditions

Re	p_0 (kPa)	*A* (kPa)			*f* (kHz)	
500	6.6					
700	9.3					
3,750	49.6	$0.01p_{b0}$	$0.05p_{b0}$	$0.1p_{b0}$	30	60
7,548	99.8					
14,952	197.7					
76,631	1,013	-	-	-	-	-
153,263	2,026					

The governing equation systems that are non-dimensionalized with reference values at the reservoir condition are mapped from the physical plane into a computational plane of a general transform. To close the governing equations, standard k-ε model [10] is employed in computations. A third-order TVD (Total Variation Diminishing) finite difference scheme with MUSCL [11] is used to discretize the spatial derivatives, and a second order-central difference scheme for the viscous terms, and a second-order fractional step method is employed for time integration.

2.2 Computational Conditions

Figure 1 shows an ISO-type toroidal throat sonic Venturi nozzle [12] used in the present study. The radius of curvature at the throat of the nozzle is twice the throat diameter ϕD (= 0.5935 mm). The straight divergent part has a half angle of θ = 3° and its axial length is 3.0D. In order to simulate the pressure disturbance downstream, a sudden enlargement section that is 30D long and 30D high is connected to the nozzle exit. The nozzle inlet is located at 100D upstream of the nozzle throat.

In the steady computations, the total pressure p_0 (reservoir) and back pressure p_{b0} are given at the inlet and outlet of the critical nozzle, respectively. The back pressure p_{b0} is kept constant at 0.5p_0 and the inlet total pressure p_0 is varied to change the Reynolds number. Ranges of Reynolds number are from 500 to 153,263 (Table 1). Total temperature is T_0 = 298K.

In order to simulate the effects of pressure disturbance on the critical flows, a sinusoidal wave with an amplitude A, an angular frequency ω (= $2\pi f$) and a phase φ is assumed at the exit of the sudden enlargement section as illustrated in Fig.1. As shown in this figure, point A is located at -0.1D upstream of nozzle throat and points B, C and D are located at 0.5D, 2.0D and 3.0D downstream of the nozzle throat, respectively. Combinations of A and f used in the present simulation are shown in Table 1.

3. RESULTS AND DISCUSSIONS

3.1 Flow Characteristics in Case without Pressure Disturbance

Figures 2 show the effects of temperature and pressure on the compressibility factor Z. If the gas is assumed to be an ideal gas, the compressibility factor is 1.0, regardless of pressure. As seen from this figure, the

virial equation of state predicts a monotonous change in Z with pressure. Modified Berthelot's equation of state gives similar results with the virial equation of state for air gas. In the present study, modified Berthelot's equation of state is selected to simulate the air gas through the critical nozzle because it exhibits better agreement with the virial equation of state.

In Fig. 3, the present computations are validated with the experimental results [13] using air gas in which the Reynolds number is based on the diameter of the nozzle throat and the total properties at the inlet of the nozzle. It is known that the coefficient of discharge is a strong function of the Reynolds number, and the predicted coefficients of discharge are in good agreement with the experimental results below *Re*=14,952. It is believed that the present computational method effectively predicts the gas flow through the critical nozzle for low Reynolds number.

Furthermore, noticeable trend in the coefficient of the discharge can be found in the range of Reynolds numbers above 14,952 for air, where the coefficient of the discharge decreases with an increase in Reynolds number. This obviously differs from the trend that has reported by many researchers [16–18]. A similar trend is found in Johnson's data for hydrogen gas [19].

For an ideal gas assumption, the present computational results predict the coefficient of the discharge, which increases with the Reynolds number and then approaches a certain constant value [20]. However, the present computation taking into account the real gas effect is qualitatively similar to results

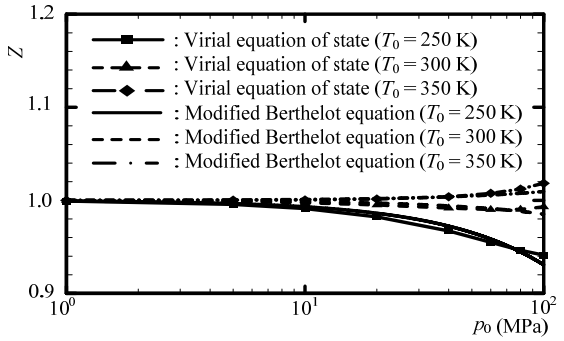

Fig 2. Comparison of the equation of state

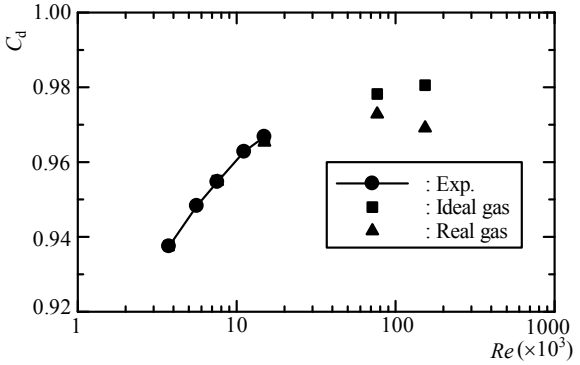

Fig 3. Effect of Reynolds number on discharge coefficient

obtained by Johnson [19] and Nakao [2]. Unfortunately, a clear and persuasive reasoning for this is, at present, not known. Such a trend in the discharge coefficient can give rise to a significant error in the mass flow at high-pressure conditions. More studies are needed to elucidate this ambiguous problem.

Figure 4 shows the effect of Reynolds number on the mass fluxes at the nozzle throat in the range from *Re*=7,548 to 153,263. In case of *Re* = 7,548 and 14952, the mass flux distributions for both the real and ideal gases are nearly the same. However, with an increase of Reynolds number, a little difference between ideal and real gases is mainly recognized in the region outside the boundary layer and the mass flux of real gas becomes slightly small. It is considered that a decrease of C_d with an increase of Reynolds number in case of real gas in Fig.3 may be due to the decrease of mass flux.

Figure 5 shows the axial distributions of the computed values of ratio of specific heats. Note that ratio of specific heats of ideal gas is constant at 1.4. Ratio of specific heats increases through the nozzle with an increase of Reynolds number. This variation in the ratio of specific heats with Reynolds number has a significant

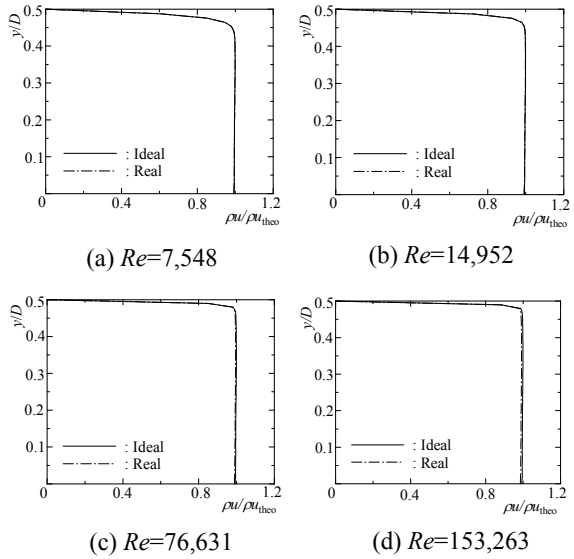

Fig 4. Comparison of average mass fluxes of ideal and real gas

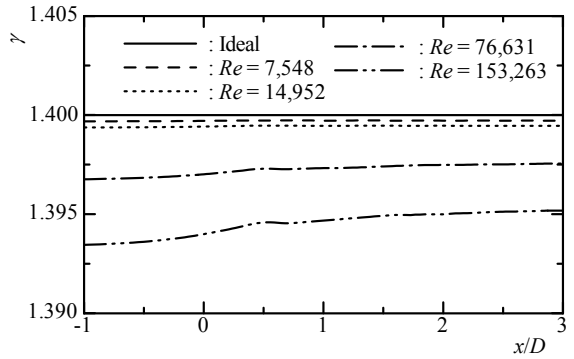

Fig 5. Effect of Reynolds number on ratio of specific heats

influence on the mass flow.

In order to investigate the real gas effects, the computed compressibility factors along the nozzle axis are shown in Fig.6. The computed compressibility factors for the real gas seem to decrease during the process of the flow to be accelerated through the nozzle throat.

3.2 Effects of Pressure Disturbance on the Flows

For unsteady computations, the pressure signal imposed on the downstream boundary is given as a sinusoidal periodic wave in the range from Re = 500 to 14,952. For the pressure fluctuation of f = 60 kHz (A = $0.01p_{b0}$, $0.05p_{b0}$, $0.1p_{b0}$), the computed pressure-time histories at the measuring point A on the nozzle wall are shown in Fig. 7. Figures 7(a) and 7(b) are pressure-time histories for Re = 700 and 3,750, respectively, and p_{av} means the time-mean local static pressure.

For Re = 700, the static pressures fluctuate with time and they are quite periodic. Furthermore, it is found that the unsteady effects of the pressure fluctuations can propagate upstream of the throat of the critical nozzle. Amplitude becomes large with an increase of A. For Re = 3,750, fluctuations in the static pressure are not observed for all cases. The fluctuations of static pressure for Re = 500 was similar tendency to result of Re = 700. For Re = 7,548 and 14,952, they showed similar tendency to result of Re = 3,750.

Figures 8 shows pressure-time histories at point A for f = 30 kHz. Figures 8(a) and 8(b) are pressure-time histories for Re = 700 and 3,750, respectively. As seen from these figures, in case of the pressure disturbance with large amplitude and small frequency, the pressure fluctuations could propagate upstream of the nozzle throat. Similar tendency is obtained in the range from Re = 500 and 14,952.

Figures 9 and 10 show time-dependent sonic lines of the flow through the critical nozzle for f = 60 kHz in cases of Re = 700 and 3,750, respectively (A = $0.01p_{b0}$, $0.05p_{b0}$, $0.1p_{b0}$). In Fig.9, the sonic line fluctuations are slightly observed with an increase of amplitude. However, for Re = 3,750 (Fig.10), it is found that the sonic line close to the throat do not fluctuate for three amplitude.

Figures 11 and 12 show time-dependent sonic lines for f = 30 kHz in cases of Re = 700 and 3,750, respectively (A=$0.01p_{b0}$, $0.05p_{b0}$, $0.1p_{b0}$). In Fig.11, a considerable amount of excursion of the sonic line is found near the nozzle throat for three amplitudes. The sonic lines appear highly distorted and they strongly depend on time. However, for Re = 3,750 (Fig.12), it is found that the sonic line downstream of the nozzle throat fluctuates largely for A = $0.01p_{b0}$ and $0.05p_{b0}$.

Figures 13(a) and 13(b) show the computed mass flow rate fluctuations for f = 60 kHz in cases of Re = 700 and 3,750, respectively. Here $\dot{m}_c$ means the time-mean mass flow rate that is obtained from the steady computations

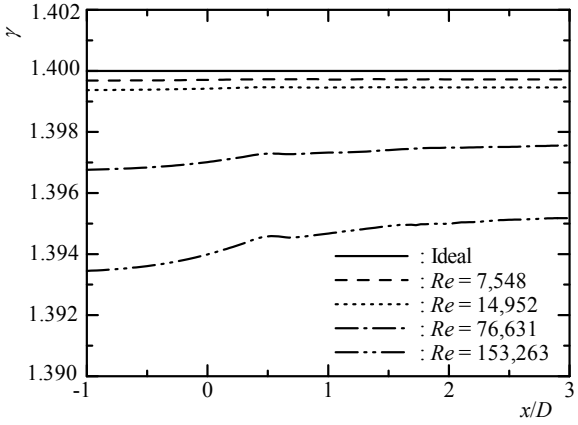

Fig 6. Effect of Reynolds number on compressibility factor

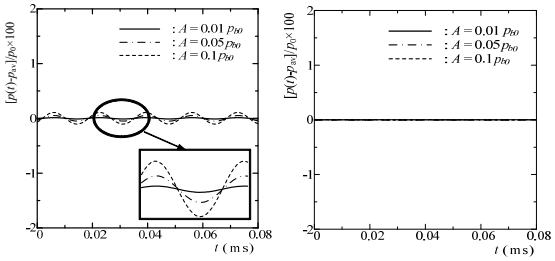

(a) Re=700 (b) Re=3,750

Fig 7. Pressure-time histories at point A (f = 60 kHz)

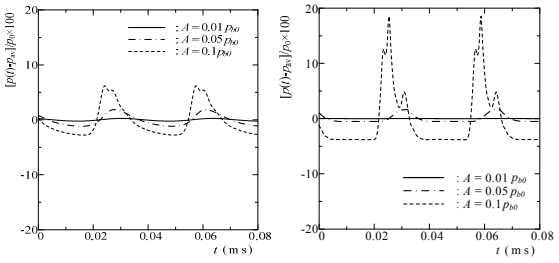

(a) Re=700 (b) Re=3,750

Fig 8. Pressure-time histories at point A (f = 30 kHz)

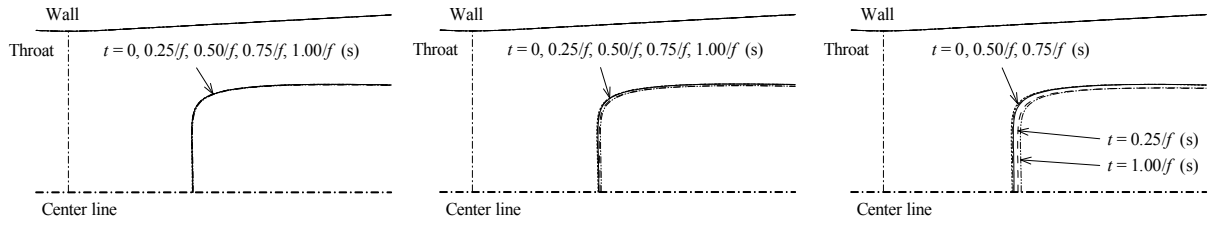

(a) A=$0.01p_{b0}$ (b) A=$0.05p_{b0}$ (c) A=$0.1p_{b0}$

Fig 9. Time dependent sonic lines (Re = 700, f = 60 kHz)

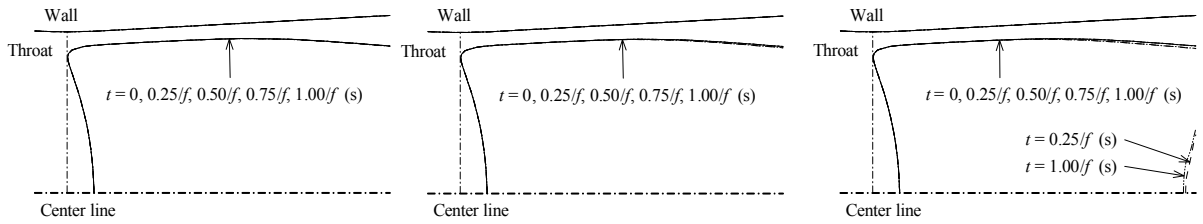

(a) A=0.01p_{b0} (b) A=0.05p_{b0} (c) A=0.1p_{b0}

Fig.10 Time dependent sonic lines (Re = 3,750, f = 60 kHz)

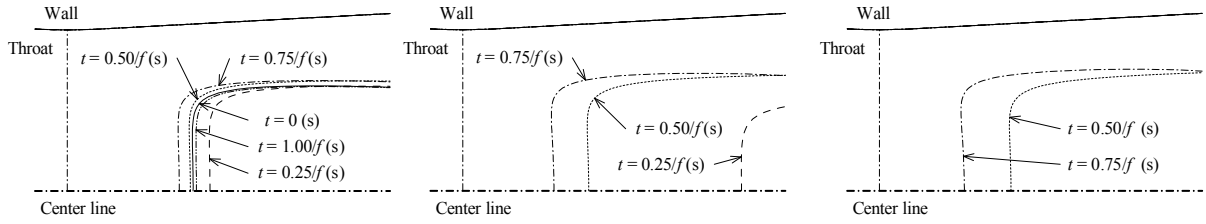

(a) A=0.01p_{b0} (b) A=0.05p_{b0} (c) A=0.1p_{b0}

Fig.11 Time dependent sonic lines (Re = 700, f = 30 kHz)

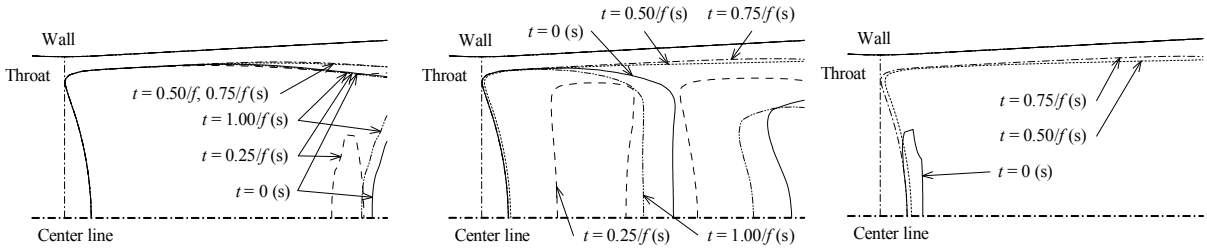

(a) A=0.01p_{b0} (b) A=0.05p_{b0} (c) A=0.1p_{b0}

Fig.12 Time dependent sonic lines (Re = 3,750, f = 30 kHz)

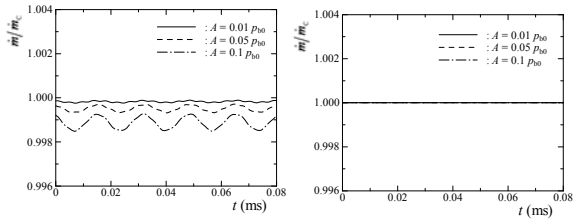

(a) Re =700 (b) Re =3,750

Fig.13 Mass flow rate fluctuation with time (f=60kHz)

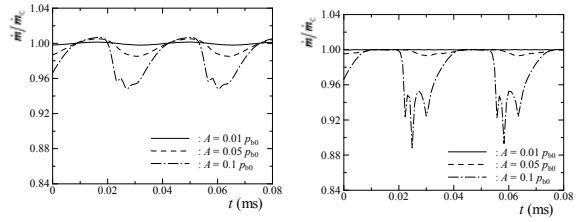

(a) Re =700 (b) Re =3,750

Fig.14 Mass flow rate fluctuation with time (f=30kHz)

for each Reynolds number. It is found for Re = 700 (Fig.13(a)) that the mass flow rate for three amplitudes fluctuates even under the condition of flow choking. The mass flow rate becomes large with an increase of amplitude. However, the mass flow rate is constant for Re = 3,750.

Figures 14(a) and 14(b) show the computed mass flow rate fluctuations for f = 30 kHz in cases of Re = 700 and 3,750, respectively. It is found that the fluctuation of the mass flow rate for A = 0.05p_{b0}, 0.1p_{b0} becomes large compared with cases of f = 60 kHz.

4. CONCLUSIONS

A computational study has been made to investigate the flow features of air through the critical nozzle. In order to simulate the real gas effects which appear at high-pressure conditions, modified Berthelot's equation of state has been employed for air and incorporated into the axisymmetric, compressible Navier–Stokes equations. The results obtained are as follows : Mass fluxes of real gas became small compared with ideal gas with an increase of Reynolds number. The coefficient of discharge of real gas through the critical nozzle decreased with an increase of Reynolds number. In high Reynolds number, the thermodynamics properties of real gas, such as the compressibility factor and the ratio of specific heats changed compared with ideal gas.

For low Reynolds number (Re = 500, 700), the unsteady effects of the pressure fluctuations could propagate upstream of the nozzle throat and it had effect on thereby fluctuations in mass flow rate through the critical nozzle. In case of the pressure disturbance with large amplitude for high Reynolds number (Re = 3,750, 7,548, 14,952), the pressure fluctuations could not propagate upstream of the nozzle throat. However, in case of the pressure disturbance with large amplitude and small frequency, the pressure fluctuations could propagate upstream of the nozzle throat.

5. REFERENCES

1. Tang, S. P. and Fenn, J. B., 1978, "Experimental determination of the discharge coefficients for critical flow through an axisymmetric nozzle", Am. Inst. Aeronaut. Astronaut. J., vol.16, no.1, pp.41-46.
2. Nakao, S., Yokoi, Y. and Takamoto, M., 1996, "Development of a calibration facility for small mass flow rates of gas and uncertainty of a sonic Venturi transfer standard", J. Flow Measmt Instrumentation, vol.7, pp.77-83.
3. Nakao, S., Irayama, T. and Takamoto, M., 2000, "Relations between the discharge coefficients of the sonic Venturi nozzle and kind of gases", J. Japan Soc. Mech. Engrs, Ser. B, vol.66, no.642, pp.438-444.
4. Johnson, R. C., 1965, "Real - gas effects in critical - flow - through nozzles and tabulated thermodynamic properties", NASA TN D-2565.
5. McCarty, R. D. and Weber, L. A., 1972, "Thermophysical properties of parahydrogen from the freezing liquid line to 5000R for pressures to 10,000 Psia", NBS TN 617.
6. McCarty, R. D.,Hord, J., and Roder,H.M, 1981, "Selected properties of hydrogen (engineering design data) ", NBS MN 168.
7. McCarty, R. D., 1975, "Hydrogen technological surveythermophysical properties", NASA SP 3089.
8. Nakao, S., 2005, "Development of critical nozzle flow meter for high pressure hydrogen gas flow measurements", In Proceedings of JSME, Fluid Dynamics Section, Kanazawa, Japan, G201.
9. Computational chemistry list, ltd. "Equations of State". CCL. NET, available from < http : // www.ccl.net / cca / documents / dyoung / topics-orig/eq_state.html >, (accessed 2008-11).
10. Launder, B. E. and Spalding , D. B., 1974, "Computer Methods in Applied Mechanics and Engineering", vol.3, pp.269-289.
11. Yee, H.C., 1989, "A class of high-resolution explicit and implicit shock capturing methods", NASA TM-89464.
12. ISO 9300, (1990).
13 Nakao, S., 2001, "A Study on the Conversion Factor of Sonic Venturi Nozzles", Proc. of NCSL International Workshop & Symposium.
16. Bignell,N.,1996, "The use of small sonic nozzles at low Reynolds numbers", Flow Meas. Instrum., Vol.7, pp.77–83.
17. Choi,Y. M., Park,K. A., Park, J. T., Choi, H. M., and Park, S. O., 1999, "Interference effects of three sonic nozzles of different throat diameters in the same meter tube", Flow Meas. Instrum., Vol.10, pp.175–181.
18. Kim, H. D., Kim, J. H., Park, K. A., Setoguchi, T., and Matsuo, S., 2004, "Study of the effects of unsteady downstream conditions on the gas flow through a critical nozzle", Proc. Instn Mech. Engrs, Part C: J. Mechanical Engineering Science, Vol.218, No.10, pp.1163–1173.
19. Johnson, R. C., 1965, "Real-gas effects in critical - flow - through nozzles and tabulated thermodynamic properties", NASA TN D-2565.
20. Kim,H.D., Kim, J. H., Park,K. A., Setoguchi,T. and Matsuo, S., 2003, "Computational study of the gas flow through a critical nozzle", Proc. InstnMech. Engrs,Part C: J.Mechanical Engineering Science, Vol.217, No.10, pp.1179–1189.

6. NOMENCLATURE

Symbol	Meaning	Unit
A	Cross-section area	(m^2)
C_d	Discharge coefficient	(-)
C_p	Specific heat at constant pressure	(J/kg·K)
D	Diameter of the critical nozzle throat	(m)
$\boldsymbol{E}$, $\boldsymbol{F}$	Inviscid flux vectors	(-)
E_t	Total energy per unit volume	(J/m^3)
$\boldsymbol{H_1}$	Source term for axsimmetry	(-)
$\boldsymbol{H_2}$	Source term for Turbulence	(-)
L	Characteristic length	(m)
$\boldsymbol{J}$	Jacobian	(-)
$\dot{m}$	Mass flow rate	(kg/s)
p	Pressure	(Pa)
p_b	Back pressure	(Pa)
R	Radius of the critical nozzle	(m)
$\boldsymbol{R}$, $\boldsymbol{S}$	Viscous flux vectors	(-)
Re	Reynolds number	(m)
T	Temperature	(K)
t	Time	(s)
$\boldsymbol{U}$	Conservative vector	(-)
u, v	Velocity components	(m/s)
v	Specific volume	(m^3/kg)
x, y	Cartesian coordinates	(m)
Z	Compressibility factor	(-)
Greeks		
γ	Ratio of specific heats	(-)
κ	Thermal conductivity	(W/m·K)
ρ	Density	(kg/m^3)
τ	Shear stress	(Pa)
θ	Angle of attack	(°)
Subscripts		
0	Stagnation point	
c	Critical point	
theo	theory	

7. MAILING ADDRESS

Mamun Mohammad
Dept. of Mechanical Engineering,
BUET, Dhaka-1000,Bangladesh.